Influence of instantaneous mode competition on the dynamics of semiconductor lasers

メタデータ	言語: eng
	出版者:
	公開日: 2017-10-03
	キーワード (Ja):
	キーワード (En):
	作成者:
	メールアドレス:
	所属:
URL	http://hdl.handle.net/2297/6701

Influence of Instantaneous Mode Competition on the Dynamics of Semiconductor Lasers

Moustafa Ahmed, *Member, IEEE,* and Minoru Yamada, *Member, IEEE*

Abstract—Comprehensive theoretical investigations of influence of instantaneous mode-competition phenomena on the dynamics of semiconductor lasers are introduced. The analyzes are based on numerical simulations of the multimode rate equations superposed by Langevin noise sources that account for the intrinsic fluctuations associated with the spontaneous emission. Numerical generation of the Langevin noise sources is performed in such a way as to keep the correlation of the modal photon number with the injected electron number. The gain saturation effects, which cause competition phenomena among lasing modes, are introduced based on a self-consistent model. The effect of the noise sources on the mode-competition phenomena is illustrated. The mode-competition phenomena induce instantaneous coupling among fluctuations in the intensity of modes, which induce instabilities in the mode dynamics and affect the state of operation. The dynamics of modes and the characteristics of the output spectrum are investigated over wide ranges of the injection current and the linewidth enhancement factor in both AlGaAs–GaAs and InGaAsP–InP laser systems. Operation is classified into stable single mode, stable multimode, hopping multimode, and jittering single mode. Based on the present results, the experimental observations of multimode oscillation in InGaAsP–InP lasers are explained as results of the large value of the linewidth enhancement factor.

Index Terms—Asymmetric gain, lasing mode, mode competition, multimode, noise, numerical modeling, semiconductor lasers.

I. INTRODUCTION

THE SEMICONDUCTOR laser displays several types of nonlinear effects. Mode-competition phenomena are caused by nonlinear gain suppression effects and are characterized by the corresponding saturation coefficients [1]–[5]. The gain suppression effect among different lasing modes is stronger than the suppression effect for an identical mode in principle when the laser supports only the fundamental transverse mode [6], [7]. The latter effect is called self-saturation, and the former one is called cross-saturation. Single-longitudinal-mode operation under CW (continuous wave) operation is achieved with help of the cross-saturation effect in lasers made of AlGaAs–GaAs [7]–[10]. Furthermore, not only symmetric but also asymmetric-type profiles for the wavelength dispersion have been found as the cross-saturation

effects, especially in long-wavelength InGaAsP–InP systems lasers [11]–[13]. It is also experimentally reported that getting the single mode operation in the long-wavelength lasers is not easy [12], [14], [15]. This inferior property is seemed to be due to the asymmetric gain saturation because of the large values of the linewidth enhancement factor (α) in long-wavelength lasers [13]. However, this inferior property has not been yet explained theoretically, which may be because the asymmetric gain saturation was ignored in most previous reports on laser dynamics [14], [16]–[18].

On the other hand, semiconductor lasers show several types of extra noise, such as hopping noise [2], [19], [20] and optical feedback noise [2], [21]–[25]. These types of noise have been explained as results of dynamic behavior of the mode- competition phenomena [2], [26]. In the case of optical feedback noise, the lasing modes are formed not only by the laser cavity itself, but also by the external cavity formed by space between the laser and a connected device such as the optical fiber or the optical disc [25]. The intrinsic seeds of the noise are fluctuations in the electron and photon numbers associated with the electron transitions between the conduction and the valence bands, and are counted in terms of Langevin noise sources in the rate equations. The noise characteristics have been well explained by means of small-signal analysis in which time variations of the electron and photon numbers as well as the Langevin noise sources are transformed into frequency components [27].

In most previous work on mode-competition phenomena, the intensity fluctuations were assumed to be not sufficiently large to change the operation state [2], [4], [20]. However, the fluctuations of mode intensities can change the state of operation as pointed out in [18]. Description of such a change of the operation state becomes possible by performing time-dependent analysis of the mode-competition phenomena and tracing the time variation of the laser operation. We have recently formulated a new model of numerical analysis of the multimode rate equations in which both gain saturation effects and the Langevin noise sources are introduced [26]. However, detailed examinations of the mode-competition phenomena and their influence on the laser operation were lacking.

In this paper, we apply our multimode model [26] to investigate in detail the effect of the linewidth enhancement α-factor and the Langevin noise sources on mode-competition phenomena in both the AlGaAs and InGaAsP laser systems. The corresponding variations of the state of laser operation, the time-averaged output spectrum, and the induced noise are also examined.

This paper is organized as follows. In the next section, we introduce our multimode model for simulating the dynamics

of the lasing modes in detail. The introductions of the gain saturation effects into the rate equations of the modal photon number and the injected electron number are explained, and a generalized model for simulating the associated Langevin noise sources is presented. In Section III, we present an illustration of the influence of the Langevin noise sources on the mode-competition phenomena based on a two-mode model. In Section IV, the results of investigating the influence of the instantaneous-mode competition on dynamics of the modes and the time-averaged output spectrum are shown. The analyzes are performed over wide ranges of the injection current and the linewidth enhancement α-factor for both AlGaAs–GaAs and InGaAsP–InP lasers. Four possible states of operation are pointed out: namely the "stable single mode," "stable multimode," "jittering single mode," and "hopping multimode." Characterization of the relative intensity noise (RIN) in these states of mode operation is presented. Conclusions of this work are given in Section V.

II. THEORETICAL MODEL

A. Multimode Rate Equations

The nonlinear dynamics of the lasing modes are described mathematically by multimode rate equations of the photon number S_p of the lasing modes and the injected electron number N

$$\frac{dS_p}{dt} = [G_p - G_{th}]S_p + C_p \frac{N}{\tau_s} + F_p(t) \qquad (1)$$

$$\frac{dN}{dt} = -\sum_p A_p S_p - \frac{N}{\tau_s} + \frac{I}{e} + F_N(t) \qquad (2)$$

where $p = 0, \mp 1, \mp 2, \ldots, \mp M$ is the mode number and G_p is the optical gain of mode p. The mode $p = 0$ with wavelength λ_0 is assumed to lie at the center of the spectral profile of the gain. The lasing modes on the long-wavelength side of the central mode of the gain profile $\lambda_p > \lambda_0$ are indicated with positive numbers, $0 < p \leq M$, while the modes on the shorter side, $\lambda_p < \lambda_0$, are indicated with negative numbers $-M \leq p < 0$. That is

$$\lambda_p = \lambda_0 + p\Delta\lambda \qquad (3)$$

where $\Delta\lambda = \lambda_0^2/n_r L$, with n_r and L as the refractive index and length of the active region, is the mode wavelength spacing. G_{th} is the threshold gain level, and is determined by the loss coefficient κ of the laser and the mirror loss

$$G_{th} = \frac{c}{n_r} \left\{ \kappa + \frac{1}{2L} \ln \frac{1}{R_f R_b} \right\} \qquad (4)$$

where

R_f, R_b power reflectivities at the front and back facets, respectively;
τ_s lifetime of the electron for spontaneous emission;
e electron charge;
I injection current.

Based on applying a third order-perturbation approach to analyze the optical gain in the density-matrix analysis, the modal gain is described by [5], [6]

$$G_p = A_p - BS_p - \sum_{q \neq p} \left\{ D_{p(q)} + H_{p(q)} \right\} S_q \qquad (5)$$

where

A_p first-order (or the linear) gain coefficient;
B self-saturation coefficient;
$D_{p(q)}, H_{p(q)}$ coefficients for the cross-saturation effects of gain.

These coefficients are given as [5], [6]

$$A_p = \frac{a\xi}{V} \{N - N_g - bV(\lambda_p - \lambda_0)^2\} \qquad (6)$$

$$B = \frac{9}{2} \frac{\pi c}{\varepsilon_o n_r^2 \hbar \lambda_0} \left(\frac{\xi \tau_{in}}{V} \right)^2 a|R_{cv}|^2 (N - N_s) \qquad (7)$$

$$D_{p(q)} = \frac{4}{3} \frac{B}{\left(\frac{2\pi c \tau_{in}}{\lambda_p^2} \right)^2 (\lambda_p - \lambda_q)^2 + 1} \qquad (8)$$

$$H_{p(q)} = \frac{3}{4} \left(\frac{a\xi}{V} \right)^2 (N - N_g)$$
$$\cdot \frac{\frac{1}{\tau_s} + \frac{3}{2} \frac{a\xi}{V} S + \alpha \frac{2\pi c}{\lambda_p^2} (\lambda_q - \lambda_p)}{\left(\frac{1}{\tau_s} + \frac{3}{2} \frac{a\xi}{V} S \right)^2 + \left(\frac{2\pi c}{\lambda_p^2} \right)^2 (\lambda_q - \lambda_p)^2} \qquad (9)$$

where a is the so-called slope (or tangential) coefficient to give the local linear gain, b is a coefficient giving the wavelength dispersion of the linear gain, N_g is the transparent electron number, R_{cv} is the dipole moment, τ_{in} is the intraband relaxation time, N_s is an electron number characterizing the saturation coefficient B, V is the volume of the active region, ξ is the field confinement factor into the active region, c is the speed of light in free space, and α is the so-called linewidth enhancement factor, which describes the simultaneous variation of the optical gain and the refractive index with changes in the electron number [28]. $S = \sum_p S_p$ is the total photon number. The form of $H_{p(q)}$ in (9) can be simplified for large modal separation

$$\frac{1}{\tau_s} + \frac{3}{2} \frac{a\xi}{V} S \ll \frac{2\pi c}{\lambda_p^2} |\lambda_q - \lambda_p|$$

to obtain the relation

$$H_{p(q)} \approx \frac{3\lambda_p^2}{8\pi c} \left(\frac{a\xi}{V} \right)^2 \frac{\alpha(N - N_g)}{\lambda_q - \lambda_p}. \qquad (10)$$

Since the coefficient $D_{p(q)}$ gives similar values for wavelength differences of $\lambda_p - \lambda_q$ and $\lambda_q - \lambda_p$, $D_{p(q)}$ is called the symmetric cross-saturation coefficient. On the other hand, equation (10) indicates that the coefficient $H_{p(q)}$ is inversely proportional to $\lambda_q - \lambda_p$. Therefore, $H_{p(q)}$ works to suppress the lasing gain for the modes on the short-wavelength side: $H_{p(q)} > 0$ for $\lambda_p < \lambda_q$, but works to enhance the lasing gain of the modes on the longer wavelength side: $H_{p(q)} < 0$ for $\lambda_p > \lambda_q$. Thus, $H_{p(q)}$ is called the asymmetric cross-saturation coefficient [1], [4], [5]. The effect of $H_{p(q)}$ is pronounced at high injection levels with large values of the linewidth enhancement α-factor.

It is worth noting that, in rate equation (2), N corresponds to the injected density of electrons $n = N/V$, which is determined

by the zeroth-order terms of the density matrix in the conduction and valence bands, as given by the third-order perturbation approach in [5], [29]. The linear and nonlinear gain coefficients are determined from these zeroth-order terms, or equivalently N as given in the above equations.

Inclusion of the spontaneous emission into the lasing mode p is described in terms of the spontaneous emission factor C_p, which is given as [25]

$$C_p = \frac{a\xi\tau_s/V}{[2(\lambda_p - \lambda_0)/\delta\lambda]^2 + 1} \tag{11}$$

where $\delta\lambda$ is the half width of the spontaneous emission profile.

The terms $F_p(t)$ and $F_N(t)$ in (1) and (2) are Langevin noise sources and are added to the rate equations to trigger fluctuations in the modal photon numbers and the electron number. The noise sources are uncorrelated among the lasing modes, but have cross-correlation between the modal photon number and the electron number as follows:

$$\langle F_p(t)F_q(t')\rangle = V_{pq}\delta_{pq}\delta(t - t') \tag{12}$$
$$\langle F_N(t)F_N(t')\rangle = V_{NN}\delta(t - t') \tag{13}$$
$$\langle F_p(t)F_N(t')\rangle = V_{pN}\delta(t - t') \tag{14}$$

where $\delta(t-t')$ is Dirac's δ function and δ_{pq} is Kronecker's delta for p and q. The coefficients V_{pq}, V_{NN}, and V_{pN} are variances of the noise sources. The determination of these variances and numerical generation of the noise sources will be shown in the next subsection.

B. Generation of Langevin Noise Sources

In the computation of the laser dynamics, the noise sources are generated with the aid of the computer random number sources. However, these random generations should satisfy the correlation relations (12)–(14) among the noise sources. In previous works [26], [30], the authors proposed a technique to solve this problem and adopt these numerical generations for both cases of single mode and multimode operations. In this subsection, we apply such a technique to the present model. The basic idea of the technique is to transform the original set of rate equations (1) and (2) to a new set in which the rate equation of the electron number is replaced by the following equation [26]:

$$\frac{d}{dt}\left\{N + \sum_p k_p S_p\right\}$$
$$= -\sum_p A_p S_p - \frac{N}{\tau_s} + \frac{I}{e} + \sum_p k_p$$
$$\cdot \left\{\left[A_p - BS_p - \sum_{q \neq p}(D_{p(q)} + H_{p(q)})S_q - G_{th}\right]S_p\right.$$
$$\left. + C_p\frac{N}{\tau_s}\right\} + \left\{F_N(t) + \sum_p k_p F_p(t)\right\}. \tag{15}$$

Here, the transformed noise source $F_N(t)+\sum_p k_p F_p(t)$ is constructed in such a way as to orthogonalize with respect to the source $F_q(t)$ associated with the photon number of mode q, i.e.,

$$\left\langle\left\{F_N(t) + \sum_p k_p F_p(t)\right\}F_q(t')\right\rangle = 0. \tag{16}$$

A newly introduced parameter k_p is evaluated by help of (12) and (16) to be

$$k_p = -\frac{\langle F_p(t)F_N(t')\rangle}{\langle F_p(t)F_p(t')\rangle}. \tag{17}$$

Other equations for the modal photon numbers S_p are used in the new set with the original forms of (1).

In the numerical calculation, the noise sources are given at sampling time t_i as

$$F_p(t_i)=\sqrt{\frac{V_{pp}(t_i)}{\Delta t}}\,g_p, \tag{18}$$

$$F_N(t_i)+\sum_p k_p(t_i)F_p(t_i)=\sqrt{\frac{V_{NN}(t_i)+\sum\limits_p k_p(t_i)V_{pN}(t_i)}{\Delta t}}\,g_N, \tag{19}$$

where $\Delta t = t_{i+1} - t_i$ is a step in the time variation, and g_p and g_N are independent Gaussian random numbers with zero mean values and variances of unity. The variances of the noise sources at each sampling time t_i are given by the mean values of S_p and N at the preceding time t_{i-1}, assuming quasi-steady sates $(dS_p/dt \approx dN/dt \approx 0)$ over the interval Δt [17], [26]:

$$V_{pp}(t_i)=2\left[\frac{a\xi}{V}S_p(t_{i-1}) + \frac{C_p}{\tau_s}\right]N(t_{i-1}), \tag{20}$$

$$V_{NN}(t_i)=2\left[\frac{1}{\tau_s} + \frac{a\xi}{V}\sum_p S_p(t_{i-1})\right]N(t_{i-1}) \tag{21}$$

$$V_{pN}(t_i)=-\frac{a\xi}{V}[N(t_{i-1})+N_g]S_p(t_{i-1}) - C_p\frac{N(t_{i-1})}{\tau_s}. \tag{22}$$

The parameter $k_p(t_i)$, defined in (17), is then given with the variances of the corresponding correlation functions,

$$k_p(t_i) = -\frac{V_{pN}(t_i)}{V_{pp}(t_i)}. \tag{23}$$

Finally, the noise sources associated with the electron number $F_N(t_i)$ are evaluated from the following combination of noise sources:

$$F_N(t_i) = \left\{F_N(t_i) + \sum_p k_p(t_i)F_p(t_i)\right\} - \sum_p k_p(t_i)F_p(t_i). \tag{24}$$

III. EFFECT OF THE LANGEVIN NOISE SOURCES ON THE MODE-COMPETITION PHENOMENA

Characterization of the mode-competition phenomena with the gain saturation effects can be understood with the simple case of two-mode competition [2]. The effect of the Langevin
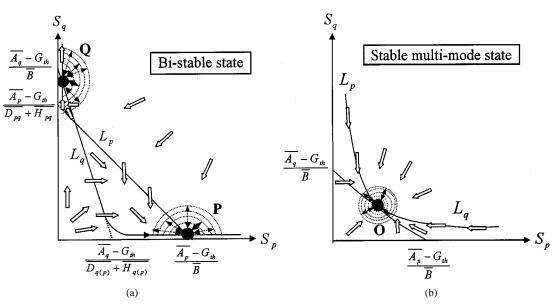
Fig. 1. Schematic diagrams of two-mode competition with counting the noise sources corresponding to: (a) a bi-stable state and (b) a near-threshold stable multimode state. The cloud around each operating point represents its fluctuation due to the noise sources. The noise sources cause switching between the operating points P and Q in the bi-stable state, while fluctuation of the multimode operating point O is small.

noise sources on the mode-competition phenomena can be also illustrated by considering the two-mode case. Equation (2) for the modal photon number is written in the case of two modes p and q as

$$\frac{dS_p}{dt} = \left[A_p - BS_p - \{D_{p(q)} + H_{p(q)}\} S_q - G_{th}\right] S_p$$
$$+ C_p \frac{N}{\tau_s} + F_p(t)$$
$$\frac{dS_q}{dt} = \left[A_q - BS_q - \{D_{q(p)} + H_{q(p)}\} S_p - G_{th}\right] S_q$$
$$+ C_q \frac{N}{\tau_s} + F_q(t)$$

where $\lambda_q > \lambda_p$. The competition phenomena between the two modes can be understood with the help of schemes in Fig. 1(a) and (b), which correspond to bi-stable and near-threshold multimode states of operation, respectively. The lines L_p and L_q are loci of the steady-state solutions $dS_p/dt = 0$ and $dS_q/dt = 0$, i.e., $F_p(t) = F_q(t) = 0$. The straight parts of the lines are determined by the terms between the brackets in the above equations when both photon numbers S_p and S_q are large enough. On the other hand, the curved parts of the lines are caused by the inclusion of spontaneous emission. The hollow arrows indicate the flow of the operating point. The directions of the arrows are determined by the signs of dS_p/dt and dS_q/dt in each region. Fig. 1(a) is the case when the injection current I is far above the threshold current level I_{th}. The laser may work in either of the stable operating points P or Q when the fluctuation terms $F_p(t)$ and $F_q(t)$ are neglected. The saddle point, which is the cross point of lines L_p and L_q, becomes close to the operating point of mode q due to the effect of the asymmetric gain saturation. Introduction of the noise sources $F_p(t)$ and $F_q(t)$ has the effect of separating the operating points from P or Q, as schematically shown in the figure with the clouds surrounding P and Q. Fluctuations of the operating points cause jitter in the operation of either of the modes, or switching between the two operating

points when these points go over the saddle point, which is seen in experiments as hopping or jumping of lasing modes [7], [18]. The summed value of the fluctuating photon numbers $S_p + S_q$ is strongly changed, resulting in so-called mode-hopping noise [2].

Fig. 1(b) shows the case when the injection current I is near to I_{th}. In this case, S_p and S_q are so small that the saturation effects are very weak. The relative contribution of the spontaneous emission to the operation becomes large, which results in curvature of the operating lines. The operating point becomes unique as indicated by the point O, and the laser shows stable multimode operation. Fluctuations in the operating point O due to the noise sources are not large to change the state of operation in this case.

IV. NUMERICAL SIMULATION AND DISCUSSION

We perform simulations of mode dynamics by numerical integration of the rate equations (1) and (2) by means of the fourth-order Runge–Kutta algorithm. The noise sources $F_p(t)$ and $F_N(t)$ are simulated through the forms from (18)–(24). The Gaussian random numbers g_p and g_N are generated by applying the Box–Mueller algorithm [31] to a corresponding set of uniformly distributed random numbers generated by the random sources of the computer [30]. The number of modes counted in the calculation is 31, that is, $M = 15$. The integration step is $\Delta t = 10$ ps, which ensures that the noise sources have white noise characteristics up to frequencies higher than 10 GHz [32]. The integration is carried out over a period of 2.6 μs, which is long enough to determine the lasing operation. In the simulations, we artificially change the linewidth enhancement factor α over a wide range from zero (i.e., ignoring the asymmetric gain saturation) to six, which corresponds to operation of AlGaAs and InGaAsP lasers [33]. As numerical parameters in our simulation, we adopt those of the buried-heterostructure (BH) AlGaAs/GaAs lasers emitting in 0.85 μm for the range of $0 \leq \alpha \leq 3.5$. The parameters of

TABLE I

VALUES OF THE PARAMETERS USED IN THE SIMULATIONS OF BURIED HETEROSTRUCTURE 0.85-μm AlGaAs, 1.3-μm InGaAsP, AND 1.55-μm InGaAsP LASERS

Parameter	850 nm GaAs	1.3μm InGaAsP	1.55μm InGaAsP
Slope of linear gain a	2.75×10^{-12} m^{3}s^{-2}	5.84×10^{-12} m^{3}s^{-2}	6.75×10^{-12} m^{3}s^{-2}
Electron number at transparency N_g	1.89×10^8	1.01×10^8	7.38×10^7
Dispersion parameter of linear gain b	2.83×10^{19} m^{-3}A^{-2}	2.75×10^{18} m^{-3}A^{-2}	9.07×10^{17} m^{-3}A^{-2}
Dipole moment R_{cv}^2	2.8×10^{-57} C^{2}m^2	6.61×10^{-57} C^{2}m^2	9.96×10^{-57} C^{2}m^2
Electron number characterizing nonlinear gain N_s	1.53×10^8	8.09×10^7	5.92×10^7
Electron life time τ_s	2.79 ns	varied	varied
Refractive index of active region n_r	3.59	3.367	3.525
Nonradiative recombination rate A_{nr}	---	10^8 s^{-1}	10^8 s^{-1}
Radiative recombination rate B_r	---	5.0×10^{-41} m^{6}s^{-1}	7.5×10^{-41} m^{6}s^{-1}
Auger recombination rate C_{AUG}	---	1.0×10^{-16} m^{3}s^{-1}	1.5×10^{-16} m^{3}s^{-1}
Length of the active region L	300 μm		
Volume of the active region V	90 μm^3		
Field confinement factor ξ	0.2		
Intraband relaxation time τ_{in}	0.1 ps		
Half width of spontaneous emission $\delta\lambda$	23 nm		
Internal absorption κ	2000 m^{-1}		
Front facet power reflectivity R_f	0.2		
Back facet power reflectivity R_b	0.7		

BH In$_x$Ga$_{1-x}$As$_y$P$_{1-y}$/InP lasers, with $x = 0.453y$ [34], are considered for the larger values of the α-factor: lasers emitting at 1.3 μm ($y = 0.57$) are considered when $3.5 < \alpha \leq 5$, while 1.55 μm lasers ($y = 0.85$) are considered for $5 < \alpha \leq 6$. Table I lists the numerical values of the parameters used in the simulations for the three laser systems. The physical parameters of the InGaAsP materials are calculated as described in [34], while the parameters characterizing the linear and nonlinear gain: a, b, N_g, R_{cv}^2 and N_s are calculated following the third-order perturbation approach in [5]. The influence of nonradiative recombination on the spontaneous emission lifetime τ_s is taken to be [34]

$$\frac{1}{\tau_s} = A_{nr} + B_r NV + C_{AUG}(NV)^2 \qquad (27)$$

where A_{nr} and C_{AUG} are the rates of nonradiative recombination due to crystal imperfections and Auger processes, respectively, and B_r is the rate of radiative recombination. Such processes influence the laser threshold current I_{th}, which is related to τ_s through

$$I_{th} = \frac{eN_{th}}{\tau_s} \qquad (28)$$

where the electron number at threshold N_{th} is determined from G_{th} as in the following equation:

$$N_{th} = N_g + \frac{V}{a\xi} G_{th}. \qquad (29)$$

The dynamics of the lasing modes, output spectrum, and relative intensity noise (RIN) induced by mode competition are examined over wide ranges of the injection current $I = I_{th} \sim 3I_{th}$, and the linewidth enhancement factor ($\alpha = 0 \sim 6$). The output spectrum is evaluated by averaging the modal photon number over the integration time T, after the transients die out. The RIN is calculated from the fluctuations in the total photon number $\delta S(t) = S(t) - \overline{S}$, where $\overline{S}$ is the mean value of $S(t)$, over the finite time T as [30]

$$RIN = \frac{1}{\overline{S}^2} \left\{ \frac{1}{T} \int_0^T \left[\int_0^\infty \delta S(t) \delta S(t + \tau) e^{j\omega\tau} \, d\tau \right] dt \right\}$$

$$= \frac{1}{\overline{S}^2} \left\{ \frac{1}{T} \left| \int_0^T \delta S(\tau) e^{-j\omega\tau} \, d\tau \right|^2 \right\} \qquad (30)$$

where the fast Fourier transform (FFT) is applied to calculate RIN through this equation.

A. Dynamics of Laser Modes

Examples of simulation results near the threshold level are given in Fig. 2. Fig. 2(a) plots the time variation of $S_p(t)$ of the dominant modes $p = 0, -1$ and $+1$ when $\alpha = 2.8$ and $I = 1.15I_{th}$ in the period $t = 20 \sim 40$ ns with and without inclusion of the noise sources. In this case, the gain has homogeneous spectral broadening. Therefore, the modes attain similar
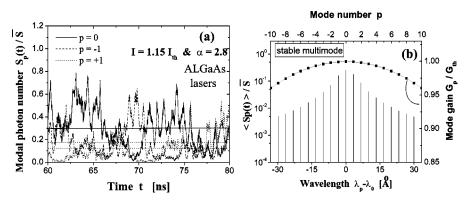
Fig. 2. Simulation results at $I = 1.15 I_{th}$ and $\alpha = 2.8$: (a) time variation of the modal photon number with and without noise sources (dc values) and (b) spectra of the photon number and gain. The modes simultaneously oscillate and the laser output indicates multimode oscillation. The gain is almost homogeneously saturated.
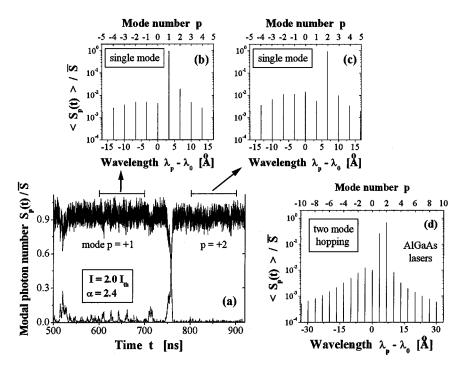

Fig. 3. Simulation results at $I = 2.0 I_{th}$ and $\alpha = 2.4$ for AlGaAs lasers: (a) time variations of the photon numbers of the dominant two modes $p = +1$ and $+2$, (b) temporal spectrum for $600 < t < 700$ ns, (c) temporal spectrum for $800 < t < 900$ ns, and (d) timely averaged spectrum. The time variations exhibit mode hopping, and the spectrum indicates that the two dominant modes carry most of the total photon number.

photon numbers in both cases of simulations and oscillate simultaneously. The simulation without noise sources results in the shown dc values of S_p, while the inclusion of noise sources induces continuous hopping of the modes with variations in time. Fig. 2(b) shows the homogeneous spectral broadening of the corresponding laser output and gain. This operation corresponds to the "stable multimode operation" that was explained with the mode-competition diagram in Fig. 1(b). Such a state of stable multimode operation is common for $0 \leq \alpha \leq 3.5$ (AlGaAs lasers), when $I < 1.29 I_{th}$. However, the upper level of I of such an operation increases up to $1.7 I_{th}$ in the case of InGaAP lasers. In these cases, the gain is almost homogeneous near the threshold level G_{th} for several modes on the long-wavelength side, and the laser emits in these modes.

An example illustrating the hopping phenomenon is shown in Fig. 3, which corresponds to conditions of $I = 2.0 I_{th}$ and $\alpha = 2.4$ (AlGaAs lasers). Fig. 3(a) plots time variations of the photon numbers $S_p(t)$ of the dominant two modes, $p = +1$ and $+2$, normalized by the mean value $\overline{S}$. The figure indicates hopping or switching of the lasing mode around $t = 750$ ns. A typical feature of the hopping phenomenon is that the switching occurs between two types of single mode oscillation, as indicated by the temporal spectra 3(b) and (c) of $S_p(t)$. These spectra are obtained by averaging $S_p(t)$ over the periods 600–700 nm and 800–900 nm, respectively. As seen in Fig. 3(b) and (c), the lasing mode is stronger than the other modes for 20 dB, which is applied as a condition of single mode oscillation. This hopping phenomenon continues for time variations in a random manner. These characteristics are then in good correspondence with the dynamics predicted by the two-mode-competition diagram in Fig. 1(a). The temporal single mode oscillations illustrated in Fig. 3(b) and (c) correspond to the operating points P and Q in Fig. 1(a), respectively. That is, the hopping is explained as instantaneous switching between two stable single mode states as
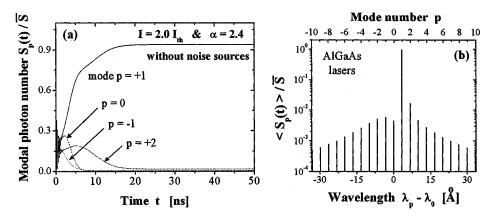
Fig. 4. Simulation results without noise sources corresponding to results in Fig. 1. The results correspond to time averaging of the single mode dynamics in the period $600 < t < 700$ ns in Fig. 3(a) and the temporal spectrum 3(b). This state of operation corresponds to one of the stable states in Fig. 1(a).
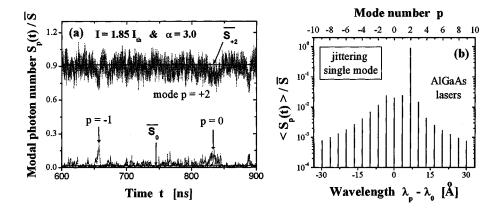

Fig. 5. Simulation results at $I = 1.85 I_{\text{th}}$ and $\alpha = 3.0$: (a) time variations of the photon numbers of the most dominant three modes with and without noise sources and (b) the output spectrum. The time variations indicate jittering of the dominant mode $p = +2$, which is not obtained by ignoring noise sources. The output spectrum proves that the laser output is almost contained in a single mode.

a result of the noise sources. The output spectrum, averaged over the total time T, shows that the total photon number S is almost contained in the two dominant modes, as shown in Fig. 3(d). We refer to this operation as "hopping multimode" in this paper.

It is helpful also to look at the corresponding results when the simulation is done without noise sources. The results are plotted in Fig. 4(a) and (b). Fig. 4(a) shows that the photon numbers of modes do not exhibit fluctuations with variation of time. Instead, they attain dc values after times as short as 15 ns. Moreover, the laser output is mainly contained in mode $p = +1$ with very large photon number compared with the side modes, as indicated by the spectrum in Fig. 4(b). It is interesting to note that these operational characteristics correspond to the single mode states in the period 600–700 ns in Fig. 3(a) and the temporal spectrum in Fig. 3(b). That is, the simulation without noise sources predicts operation in one of the two stable states in Fig. 1(a), or Fig. 3(a). The operation state in the "without noise source" case is determined by competition among the lasing modes in the transient regime, as shown in Fig. 4(a) for mode $p = +1$. Therefore, we can conclude that the mode competition is characterized not only by the asymmetric saturation of gain, but also with generation of the Langevin noise sources.

Another state of unstable operation is illustrated in Fig. 5(a) and (b), which show time variations of $S_p(t)$ of modes $p = 0, -1$ and $+2$, and the corresponding output spectrum, respectively,

at $\alpha = 3$ and $I = 1.85 I_{th}$. Fig. 5(b) indicates that the mode $p = +2$ dominates the lasing operation acquiring a time-averaged photon number higher than 20 dB of that of any side mode. That is, the condition of single mode oscillation is satisfied. However, the time variation of the modal photon number, given in Fig. 5(a), indicates instantaneous jittering among the modes, which is seen as a temporal dropout of the photon number of mode $p = +2$ associated with an increase of the photon numbers of the side modes $p = 0$ and -1. We define this state of operation to be "jittering single mode." As discussed in Section III, the jittering operation can be understood as small fluctuations of either operating points P or Q in the bi-stable state, as shown in Fig. 1(a). The instantaneous mode competition in this case is not strong enough to bring the operating point beyond the saddle point and cause mode switching. The role of the noise sources in inducing the jittering operation is also clarified by plotting the simulation results without noise sources in Fig. 5(a). As shown in the figure, only dc values are obtained and mode $+2$ dominates the lasing.

The influence of the asymmetric saturation effect on mode dynamics can be elucidated by comparing the simulation results in Fig. 3 with the results in Fig. 6, obtained by setting the α-factor to zero in (9). Fig. 6(a) indicates that competition of the side modes with the dominant mode $p = 0$ is so weak that neither mode hopping nor jittering is observed. Moreover, the
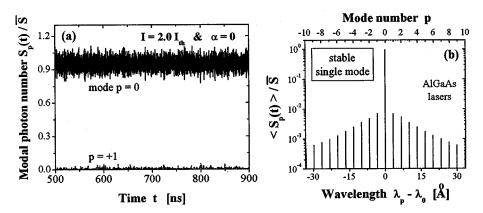
Fig. 6.   Results of simulation at $I = 2.0I_{th}$ with $\alpha = 0$: (a) time variations of the photon numbers of the dominant mode $p = 0$ and one side mode $p = +1$ and (b) the output spectrum. The central mode $p = 0$ dominates the lasing and carries most of the total photon number. This state of operation is called the "stable single mode."
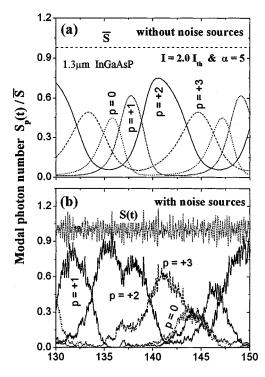

Fig. 7.   Time variations of the photon numbers of the most dominant modes at $I = 2.0I_{th}$ and $\alpha = 5.0$: (a) without noise sources and (b) with noise sources. The hopping phenomenon is so enhanced and the lasing mode is rotating among the four modes $p = 0, +1, +2,$ and $+3$.
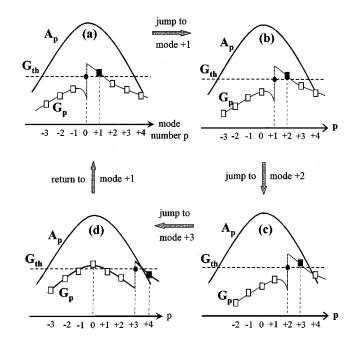

Fig. 8.   Schematic illustration of the rotation effect of the lasing frequency when the α-factor is strong. The lasing frequency jumps to the long-wavelength side modes due to the asymmetric gain saturation effect. Such mode jumping stops when the saturated gain of the central mode $p = 0$ is recovered, and the lasing frequency returns to the central mode.

output spectrum, shown in Fig. 6(b), indicates that the time-averaged photon number of mode $p = 0$ exceeds 20 dB of those of the side modes, satisfying the condition of single mode operation. In this paper, we define this state of operation to be "stable single mode."

An example of the simulation of the time variation of the modal photon number $S_p(t)$ at large values of the α-factor (InGaAsP lasers) is given in Fig. 7, which corresponds to $\alpha = 5$ and $I = 2.0I_{th}$. Fig. 7(a) and (b) plot the simulated results when the Langevin noise sources in (1) and (2) are ignored and are taken into account, respectively. Fig. 7 shows that four modes, $p = 0, +1, +2,$ and $+3$ participate in the hopping phenomenon even when the noise sources are ignored. The hopping occurs first by the central mode $p = 0$ followed by the

other modes in the order of the mode number, and then returns back to the central mode. Rotation of such a lasing mode among the hopping modes is repeated with a frequency of 88 MHz. This rotation effect of the lasing frequency cannot be explained with the two-dimensional diagram of two-mode competition in Fig. 1(a). Instead, three or higher dimensional diagrams of mode-competition are required, which is very complicated. Alternatively, the rotation effect can be understood with the help of the temporal spectra of the linear and saturated gain shown in Fig. 8(a)–(d) as follows. Fig. 8(a) corresponds to operation in the central mode $p = 0$, which is represented by the solid circle. Since the α-factor is large, the asymmetric gain saturation works to enhance the gain of the neighbor mode on the long-wavelength side, i.e., mode $p = +1$, which is represented by the solid square in the figure. When the gain G_{+1} exceeds the threshold gain G_{th}, the lasing mode jumps to mode
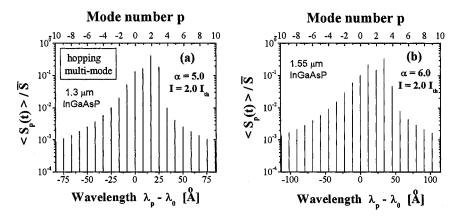
Fig. 9.   Time-averaged spectra of the modal photon number when $I = 2.0 I_{th}$ at: (a) $\alpha = 5.0$ (1.3-μm InGaAsP lasers) and (b) $\alpha = 6.0$ (1.55-μm InGaAsP lasers). The spectra are asymmetric and indicate multimode oscillation of the hopping modes.
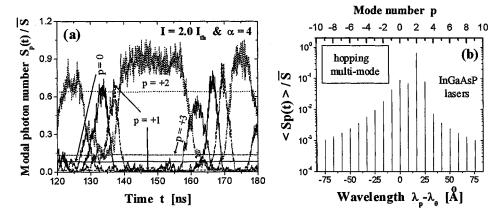

Fig. 10.   Time variations of the photon numbers of the most dominant modes at $I = 2.0 I_{th}$ and $\alpha = 4.0$ (1.3 μm InGaAsP lasers): (a) with and without noise sources and (b) the output spectrum. Ignoring the noise sources predicts stable multimode, while counting the sources fluctuates the modal gain so as to bring the rotation effect of the lasing frequency. The output spectrum is asymmetric multimode-like.

$p = +1$ and the central mode becomes a short-wavelength side mode receiving suppression from the new dominant mode, as represented in Fig. 8(b). This situation continues resulting in jumping to longer-wavelength-side modes, as given in spectra Fig. 8(c) and (d) for modes $+2$ and $+3$, respectively. However, according to (6), the linear gain of a mode becomes lower as the mode separates from the central mode $p = 0$. Thus, jumping of the lasing mode should stop at a certain mode p_{max} on the long-wavelength side; mode $+3$ in this case. At that moment, the lasing gain of the central mode $p = 0$ is recovered because its gain suppression by the mode $p_{max} = +3$ becomes small since the mode p_{max} is far from $p = 0$, and its linear gain acquires larger values $A_0 > A_{p_{max}}$, as given in (6)–(9) and illustrated in spectra 8(d). Therefore, the lasing mode hops back to the central mode $p = 0$. These steps are repeated in time. Inclusion of the noise sources causes fluctuation of the operating points, which modulates the rotation frequency. This effect is clear in Fig. 7(b), where random fluctuations occur in the intensities of the lasing modes as well as on the time interval of the mode hopping so as to decrease the rotating frequency to 42 MHz.

The corresponding time-averaged output spectrum is shown in Fig. 9(a). The figure indicates an asymmetric multimode-like output spectrum, which is in good correspondence with the spectra observed in experiments by Mito *et al.* [15] for 1.3-

and 1.5-μm BH InGaAsP–InP lasers. Increasing the current I to $2.8 I_{th}$ also results in the spectrum of multimode oscillation with a one-mode-shift of the hopping modes toward the long-wavelength side, as shown in Fig. 9(b). It is worth mentioning that such multimode spectra result from time averaging of the instantaneous single mode operation. We also refer to this operation as the "hopping multimode" in this paper. Such characteristics of strong mode hopping in InGaAsP lasers dominate the operation when I exceeds $2.0 I_{th}$.

It is worth noting that the noise sources can also stimulate the rotation effect of the lasing frequency in InGaAsP lasers even when the simulation without noise sources predicts stable multimode operation. An example of this effect is given in Fig. 10(a), which plots the time variation of $S_p(t)$ with and without noise sources when $\alpha = 4$ and $I = 2.0 I_{th}$. The stable multimode oscillation simulated without noise sources is indicated for the dc values of photon numbers of modes $p = 0$, $+1$, $+2$ and $+3$. However, the rotation effect of the lasing frequency is clear in the figure when the noise sources are counted. This case is a good example for illustrating the effect of the noise sources in fluctuating the temporal operating points of the lasing modes in such a way as to stimulate the rotation effect, as discussed above. The output spectrum under these operating conditions is also an asymmetric multimode-like spectrum, as shown in Fig. 10(b). This type of
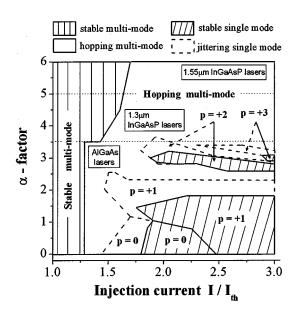
Fig. 11.   Classification of the possible states of laser operation in terms of the injection current and the α-factor. The stable single mode dominates for operation with small α-values (AlGaAs lasers), while the hopping multimode dominates for operation with large α-values (InGaAsP lasers). The operation shows stable multimode oscillation for $I < 1.29 I_{\text{th}}$ for AlGaAs lasers, and goes to a higher current $I = 1.7 I_{\text{th}}$ in InGaAsP lasers.
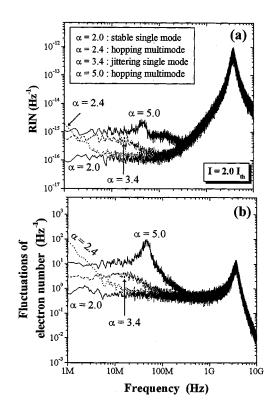

Fig. 12.   Spectral profiles of: (a) RIN and (b) fluctuations in the electron number in the investigated regions of mode operation: stable single mode ($\alpha = 2.0$), jittering single mode ($\alpha = 3.4$), and hopping multimode ($\alpha = 2.4$ and 5.0) when $I = 2.0 I_{\text{th}}$. The noise is most enhanced when the laser operates in hopping multimode and is well suppressed where the stable single mode operation is achieved.

operation characterizes InGaAsP lasers beyond the stable multimode operation for currents less than $2.0 I_{\text{th}}$.

B. Classification of Laser Operation in Terms of the α-Factor

The above results are used to classify laser operation in terms of the injection current I and the α-factor as shown as shown in Fig. 11. In each range of α that corresponds to one of the laser systems: AlGaAs (0.85 μm), InGaAsP (1.3 μm), and InGaAsP (1.55 μm), I is normalized by the corresponding threshold value I_{th}. The inclined hatched regions represent stable single mode operation, while the vertically hatched regions indicate stable multimode operation. The blank regions contoured by dashed lines represent jittering single mode operation. On the other hand, the hopping multimode state of operation is included in the blank region with the solid-line contour.

Many typical features of the dependence of laser operation on the value of the α-factor are gained from this figure. The laser operates in a stable multimode at injection levels near the threshold regardless of the α-value in AlGaAs–GaAs lasers. In the case of InGaAsP–InP lasers, the upper limit of the current I for such operation becomes higher, reaching $1.7 I_{th}$ when $\alpha = 6$ (1.55 μm InGaAsP). Stable single mode oscillation dominates for operation with small values of the α-factor, which is a typical feature of AlGaAs–GaAs lasers [7]–[10]. An increase of the α-value causes shift of the lasing mode toward the long-wavelength side and the entrance to regions of the jittering and the hopping operations. Although the stable single mode operation is obtained again for $\alpha = 3$ with $p = +2$ or $+3$, these regions are very narrow. A further increase of the α-factor brings the jittering and the hopping operations. The stable single mode operation is not obtained in InGaAsP–InP lasers, while the jittering single mode operation is found only over a narrow range of $I = 1.9 \sim 2.0 I_{\text{th}}$ around $\alpha \approx 3.6$. On the other hand, op-

eration of these lasers is dominated by the hopping multimode operation as illustrated in the figure.

C. Characterization of the RIN and Electron Number Noise

In this subsection, we characterize the spectral characteristics of the RIN of the photon number and the fluctuation in the electron number. Fig. 12(a) plots the spectral profiles of the RIN in the three states: stable single mode, jittering single mode, and hopping multimode. We include in the figure two examples of the hopping multimode operation obtained at small and large values of $\alpha = 2.4$ and 5 when $I = 2.0 I_{\text{th}}$. The high-frequency components of the RIN in all regions are almost coincident, showing the pronounced peak around the relaxation frequency of the laser. The noise-peak frequency is almost same, because it is determined by the dc values $\overline{S}$ and $\overline{N}$, which in turn are determined by the ratio I / I_{th} [35]. On the other hand, the low-frequency RIN varies over more than one order of magnitude *for variation of the α-factor* from two (stable single mode) to five (hopping multimode). The lowest level of the low-frequency RIN is obtained when the laser oscillates in the "stable single mode" state, and corresponds to the quantum fluctuations of the stable lasing mode [2]. On the other hand, the low-frequency RIN is enhanced in other regions. The maximum enhancement of the RIN occurs in the regions of multimode hopping operation. The highest RIN in the case of $\alpha = 2.4$ is shown at frequencies lower than 1 MHz, while the profile of the RIN in the case of $\alpha = 5$ peaks at a frequency around 42 MHz, which corresponds

to the frequency for switching of the hopping modes. The intensity noise in this case corresponds to the mode-hopping noise associated with switching of the lasing modes as pointed out in Sections III and IV-A. Although the level of the hopping RIN is not high in this study, it will likely be enhanced by the introduction of disturbing effects, such as a temperature change or the injection of light by external optical feedback.

The corresponding spectral characteristics of fluctuations in the electron number N are plotted in Fig. 12(b). The figure shows similar characteristics to those of the RIN. Such fluctuations cause broadening of the lasing frequency $\Delta\nu$ according to [30]

$$\Delta\nu(t) = \frac{a\xi\pi\alpha}{V}\,\delta N(t) + F_\theta(t) \tag{31}$$

where $\delta N(t)$ represents the instantaneous fluctuations in N and $F_\theta(t)$ is the Langevin noise source associated with the phase of the lasing field. The fluctuations, consequently, affect broadening of the laser linewidth Δf, which is determined as the zero-frequency component of the Fourier transform of $\Delta\nu(\tau)$ [30]

$$\Delta f = 4\pi\left[\int_0^\infty \Delta\nu(t)\Delta\nu(t+\tau)e^{j\omega\tau}\,d\tau\right]_{\omega=0}. \tag{32}$$

Therefore, the results given in Fig. 12(b) confirm that minimum broadening of the lasing frequency is obtained in the stable single mode region, while maximum broadening is induced in the hopping multimode regions.

V. Conclusion

We introduced a new study of the influence of instantaneous mode competition on the dynamics of modes of semiconductor lasers. The study was made based on performing extensive time-domain simulations when counting the Langevin noise sources. The following conclusions can be drawn.

1) The influence of the noise sources on the competition phenomena is clarified. The mode-competition phenomena are caused by the nonlinear gain saturation effects, and are instantaneously modulated by the Langevin noise sources.

2) The laser operation is classified into stable single mode, jittering single mode, stable multimode, and hopping multimode.

3) The dependencies of the laser operation on both the injection current and the linewidth enhancement factor have been investigated in both AlGaAs–GaAs and In-GaAsP–InP laser systems.

4) AlGaAs lasers operate in a stable multimode near the threshold current, while the operating conditions of the stable multimode continues up to $I = 1.7I_{th}$ for InGaAsP lasers.

5) AlGaAs lasers with small linewidth enhancement factors operate mostly in a stable single mode.

6) InGaAsP lasers do not exhibit stable single mode oscillation, but operate in a jittering single mode over a limited range of current around $\alpha = 3.6$.

7) Operation of InGaAsP lasers at high currents is characterized by rotation of the lasing mode among several long-wavelength modes and a multimode-like output spectrum. This effect, in addition to conclusion 4), fits and contributes new explanation to the experimental observations in InGaAsP–InP lasers.

8) The RIN of the photon number and the fluctuations in the electron number are enhanced in the low-frequency regime when the laser exhibits the hopping multimode.

References

[1] H. Ishikawa, M. Yano, and M. Takusagawa, "Mechanism of asymmetric longitudinal mode competition in InGaAsP/InP lasers," *Appl. Phys. Lett.*, vol. 40, pp. 553–555, 1982.

[2] M. Yamada, "Theory of mode competition noise in semiconductor lasers," *IEEE J. Quantum Electron.*, vol. QE-22, pp. 1052–1059, 1986.

[3] N. Ogasawara and R. Ito, "Longitudinal mode competition and asymmetric gain saturation in semiconductor injection lasers: I. Experiment," *Jpn. J. Appl. Phys.*, vol. 27, pp. 607–614, 1988.

[4] ——, "Longitudinal mode competition and asymmetric gain saturation in semiconductor injection lasers: II. Theory," *Jpn. J. Appl. Phys.*, vol. 27, pp. 615–626, 1988.

[5] M. Yamada, "Theoretical analysis of nonlinear optical phenomena taking into account the beating vibration of the electron density in semiconductor lasers," *J. Appl. Phys.*, vol. 66, pp. 81–89, 1989.

[6] M. Yamada and Y. Suematsu, "Analysis of gain suppression in undoped injection lasers," *J. Appl. Phys.*, vol. 52, pp. 2653–2664, 1981.

[7] ——, "A condition of single longitudinal mode operation in injection lasers with index-guiding structure," *IEEE J. Quantum Electron.*, vol. QE-15, pp. 743–749, 1979.

[8] R. F. Kazarinov, C. H. Henry, and R. A. Logan, "Longitudinal mode self-stabilization in semiconductor lasers," *J. Appl. Phys.*, vol. 53, pp. 4631–4644, 1982.

[9] M. Yamada, "Transverse and longitudinal mode control in semiconductor injection lasers," *IEEE. J. Quantum Electron.*, vol. QE-19, pp. 1365–1380, 1983.

[10] P. Liu and K. Ogawa, "Statistical measurements as a way to study mode partition in injection lasers," *J. Lightwave Technol.*, vol. LT-2, pp. 44–48, 1984.

[11] J. Manning, R. Olshansky, D. M. Fye, and W. Powazinik, "Strong influence of nonlinear gain on spectral and dynamic characteristics of InGaAsP lasers," *Electron Lett.*, vol. 12, pp. 496–497, 1985.

[12] J. Buus, *Single Frequency Semiconductor Lasers*. Bellingham, WA: SPIE, 1991.

[13] S. Ogita, A. J. Lowery, and R. S. Tucker, "Influence of asymmetric nonlinear gain on the transient of longitudinal modes in long wavelength Fabry–Perot laser diodes," *IEEE J. Quantum Electron.*, vol. 33, pp. 198–210, 1997.

[14] T. P. Lee, C. A. Burrus, J. A. Copeland, A. G. Dentai, and D. Marcuse, "Short-cavity InGaAsP injection lasers: Dependence of mode-spectra and single-longitudinal mode power on cavity length," *IEEE J. Quantum Electron.*, vol. QE-18, pp. 1101–1113, 1982.

[15] I. Mito, M. Kitamura, K. Kaede, Y. Odagiri, M. Seki, M. Sugimoto, and K. Kobayashi, "InGaAsP planar heterostructure laser diode (PBH-LD) with very low threshold current," *Electron. Lett.*, vol. 18, pp. 2–3, 1982.

[16] N. H. Jensen, H. Olesen, and K. E. Stubkjaer, "Partition noise in semiconductor lasers under CW and pulsed operation," *IEEE J. Quantum Electron.*, vol. QE-23, pp. 71–80, 1987.

[17] D. Marcuse, "Computer simulation of laser photon fluctuations: Theory of single-cavity laser," *IEEE J. Quantum Electron.*, vol. QE-20, pp. 1139–1148, 1984.

[18] M. Ohtsu, Y. Otsuka, and Y. Teramachi, "Analyzes of mode partition and mode hopping in semiconductor lasers," *IEEE J. Quantum Electron.*, vol. 25, pp. 31–38, 1989.

[19] G. Gray and R. Roy, "Noise in nearly-single-mode semiconductor lasers," *Phys. Rev. A*, vol. 40, pp. 2453–2461, 1989.

[20] M. Alalusi and R. B. Darling, "Effect of nonlinear gain on mode-hopping in semiconductor laser diodes," *IEEE J. Quantum Electron.*, vol. 31, pp. 1181–1192, 1995.

[21] G. P. Agrawal, "Effect of gain nonlinearites on periodic doubling and chaos in directly modulated semiconductor lasers," *Appl. Phys. Lett.*, vol. 49, pp. 1013–1015, 1986.

[22] M. Yamada, N. Nakaya, and M. Funaki, "Characteristics of mode-hopping noise and its suppression with the help of electric negative feedback in semiconductor lasers," *IEEE J. Quantum Electron.*, vol. QE-23, pp. 1297–1302, 1987.

[23] G. P. Agrawal and G. R. Gray, "Effect of phase-conjugate feedback on the noise characteristics of semiconductor lasers," *Phys. Rev. A*, vol. 46, pp. 5890–5898, 1992.

[24] G. R. Gray, D. Haung, and G. P. Agrawal, "Chaotic dynamics of semiconductor lasers with phase-conjugate feedback," *Phys. Rev. A*, vol. 47, pp. 2906–2015, 1994.

[25] M. Yamada, "Computer simulation of feedback induced noise in semiconductor lasers operating with self-sustained pulsation," *IEICE Trans.*, vol. E81-C, pp. 768–780, 1998.

[26] M. Ahmed, M. Yamada, and S. Abdulrhmann, "A multimode simulation model of mode-competition low-frequency noise in semiconductor lasers," *Fluct. Noise Lett.*, vol. 1, pp. L163–L170, 2001.

[27] H. Haug, "Quantum-mechanical rate equations for semiconductor lasers," *Phys. Rev.*, vol. 184, pp. 338–348, 1969.

[28] C. H. Henry, "Phase noise in injection lasers," *J. Lightwave Technol.*, vol. LT-4, pp. 298–311, 1986.

[29] Y. Suematsu and A. R. Adams, *Hand Book of Semiconductor Lasers and Photonic Integrated Circuits*.   London, U.K.: Chapman and Hall, 1994.

[30] M. Ahmed, M. Yamada, and M. Saito, "Numerical modeling of intensity and phase noises in semiconductor lasers," *IEEE J. Quantum Electron.*, vol. 37, pp. 1600–1610, 2001.

[31] A. Stuart and J. K. Ord, *Advanced Theory of Statistics*.   London, U.K.: Griffin, 1980.

[32] N. Schunk and K. Petermann, "Noise analysis of injection-locked semiconductor injection lasers," *IEEE J. Quantum Electron.*, vol. QE-22, pp. 642–650, 1986.

[33] M. Osinski and J. Buus, "Linewidth broadening factor in semiconductor lasers—An overview," *IEEE J. Quantum Electron.*, vol. QE-23, pp. 9–29, 1987.

[34] G. P. Agrawal and N. K. Dutta, *Semiconductor Lasers*.   New York: Van Nostrand Reinhold, 1993.

[35] M. Yamada, "Variation of intensity noise and frequency noise with the spontaneous emission factor in semiconductor lasers," *IEEE J. Quantum Electron.*, vol. 30, pp. 1511–1519, 1994.

Moustafa Ahmed (M'99) was born in Minia, Egypt, in 1966. He received the B.Sc. and M.Sc. degrees in physics from the Faculty of Science, Minia University, Minia, Egypt, in 1988 and 1993, respectively, and the Ph.D. Eng. degree from the Graduate School of Natural Science and Technology, Kanazawa University, Kanazawa, Japan, in 1999. His dissertation research mainly involved design methods for optical filters, and infinite-order approach to gain calculation in semiconductor lasers.

He is currently a Lecturer in the Physics Department, Minia University. Since September 2000, he has also been a Visiting Fellow at the Department of Electrical and Electronic Engineering, Kanazawa University, Kanazawa, Japan, supported by the post-doctoral program of Japan Society for Promotion of Science (JSPS). His research interests are in the areas of optoelectronics and statics and dynamics of semiconductor lasers.

Minoru Yamada (M'82) was born in Yamanashi, Japan, in 1949. He received the B.S. degree in electrical engineering from Kanazawa University, Kanazawa, Japan in 1971, and the M.S. and Ph.D. degrees in electronics engineering from the Tokyo Institute of Technology, Tokyo, Japan, in 1973 and 1976, respectively.

He joined Kanazawa University in 1976, where he is presently a Professor. From 1982 to 1983, he was a Visiting Scientist at Bell Laboratories, Holmdel, NJ. His research interests are in the areas of semiconductor injection lasers, semiconductor modulators, and unidirectional optical amplifiers.

Dr. Yamada received the Yonezawa Memorial Prize in 1975, the Paper Award in 1976, and the Achievement Award in 1978 from the IECE of Japan.